Geophysical Research Letters

RESEARCH LETTER
10.1029/2026GL122210

Asymmetric Ocean-Atmosphere Coupling Between Southeast Pacific and Southern Ocean Cooling Through Circulation and Sea-Ice Changes

Xinjia Hu[1,2], Louise J. Slater[1], Sarah M. Kang[3], and Jennifer L. Castle[2]

[1]School of Geography and the Environment, University of Oxford, Oxford, UK, [2]Climate Econometrics and Calleva Centre, Magdalen College, University of Oxford, Oxford, UK, [3]Max Planck Institute for Meteorology, Hamburg, Germany

Abstract Recent decades have seen persistent sea surface temperature (SST) cooling in the Southeast Pacific (SEP) and Southern Ocean (SO), contrasting with broad ocean warming expected under anthropogenic forcing. Using an interpretable machine-learning attribution framework applied to multi-source observations and reanalyses, we focus on monthly SST variations beyond intrinsic oceanic persistence and relate them to physical predictors. Cooling in each region is associated with distinct combinations of physical predictors. In the SO, enhanced sea-ice variability and lower-tropospheric circulation anomalies account for a substantial fraction of the post-2000 cooling. In the SEP, cooling is associated with a strengthened subtropical high, thermodynamic and cloud–radiative feedbacks. A moving-window analysis indicates asymmetric coupling, with strengthening SO-to-SEP association in SST variability and a relative decline in local SEP feedbacks. These results show how high-latitude–subtropical interactions can modulate regional SST trends under global warming through circulation, sea ice, and air–sea coupling.

Plain Language Summary Global warming is expected to raise ocean temperatures, yet parts of the Southeast Pacific and the Southern Ocean have cooled over recent decades. These regions, located near the west coast of South America and around Antarctica, are important for regulating Earth's climate and marine ecosystems. Here we analyze observations and reanalysis data from 1960 to 2024 to investigate the physical processes associated with sea surface temperature changes in these two regions. We use a data-driven approach that accounts for ocean persistence ("memory") and quantifies the additional contribution of atmospheric circulation, clouds, and sea ice. We find that cooling in the two regions arises from different local processes. In the Southern Ocean, changes in sea ice and large-scale atmospheric circulation help explain much of the recent cooling. In the Southeast Pacific, cooling is mainly linked to changes in winds, clouds, and surface heat exchange. Importantly, we also find that the connection between the two regions is uneven. Over recent decades, variability in the Southern Ocean has increasingly influenced temperatures in the Southeast Pacific, while the reverse influence has weakened. These results highlight how long-distance links between high-latitude and subtropical processes can shape regional ocean temperature trends under climate change.

Key Points:

- Interpretable machine learning method isolates physically interpretable contributors to sea surface temperature variability beyond strong oceanic persistence
- Southeast Pacific (SEP) cooling links to thermodynamics and clouds; Southern Ocean (SO) cooling relates to circulation and sea ice
- The SO-SEP linkage is stronger and more persistent in the SO-to-SEP direction than in the reverse direction, showing asymmetric coupling

Supporting Information:

Supporting Information may be found in the online version of this article.

Correspondence to:

X. Hu,
xinjia.hu@yahoo.com

Citation:

Hu, X., Slater, L. J., Kang, S. M., & Castle, J. L. (2026). Asymmetric ocean-atmosphere coupling between Southeast Pacific and Southern Ocean cooling through circulation and sea-ice changes. *Geophysical Research Letters*, *53*, e2026GL122210. https://doi.org/10.1029/2026GL122210

Received 13 FEB 2026
Accepted 27 MAY 2026

Author Contributions:

Conceptualization: Xinjia Hu, Louise J. Slater, Sarah M. Kang
Data curation: Xinjia Hu
Formal analysis: Xinjia Hu
Funding acquisition: Jennifer L. Castle
Investigation: Xinjia Hu, Sarah M. Kang
Methodology: Xinjia Hu, Louise J. Slater, Sarah M. Kang
Project administration: Jennifer L. Castle
Resources: Xinjia Hu
Supervision: Louise J. Slater
Validation: Xinjia Hu, Louise J. Slater
Visualization: Xinjia Hu
Writing – original draft: Xinjia Hu

1. Introduction

The Southern Ocean (SO: 190°–250°E, 55°–70°S) and the Southeast Pacific (SEP: 235°–290°E, 12°–28°S) are critical regions for global climate regulation, heat transport, carbon cycling, and marine productivity (Boyd et al., 2024; Gruber et al., 2023; Mayewski et al., 2009; Sallée et al., 2023). The Southern Ocean constitutes the planet's largest oceanic carbon sink, absorbing over 40% of anthropogenic CO_2 emissions (Caldeira & Duffy, 2000; Landschützer et al., 2015), while the Southeast Pacific hosts one of the world's most biologically productive upwelling systems (Pennington et al., 2006). Through coupled air–sea interactions, these regions mediate heat and carbon exchange between the deep ocean and the atmosphere, thereby shaping global climate trajectories (Armour et al., 2016; Chavez et al., 2008).

Despite ongoing greenhouse forcing, both regions have exhibited multi-decadal surface cooling since the late 20th century (Cerovečki et al., 2019; Falvey & Garreaud, 2009; Kang, Ceppi, et al., 2023). Observations reveal coherent cooling across the SEP and the Pacific sector of SO beginning in the 1980s (Figure 1), coincident with documented changes in Southern Hemisphere circulation, including trends in the Southern Annular Mode (SAM) and subtropical high-pressure systems (Garreaud et al., 2021; Marshall, 2003; Xu et al., 2022). Similar deviations from projected warming have emerged in the equatorial Pacific, where strengthened easterlies and a La Niña-like

Writing – review & editing: Xinjia Hu, Louise J. Slater, Sarah M. Kang, Jennifer L. Castle

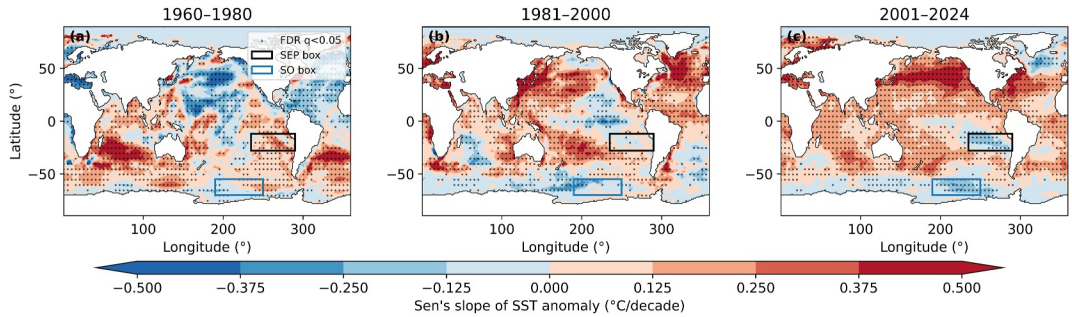

Figure 1. Sen's slope of monthly sea surface temperature anomalies (°C decade^{-1}) from HadISST1 for three periods: (a) 1960–1980, (b) 1981–2000, and (c) 2001–2024. Trends use Yue–Pilon TFPW Mann–Kendall; stippling marks grid cells significant at $q < 0.05$ after Benjamini–Yekutieli FDR. Black and blue rectangles indicate the Southeast Pacific and Southern Ocean analysis regions.

mean state have persisted despite greenhouse forcing (Qiu et al., 2024; Seager et al., 2021). These patterns suggest that large-scale circulation and polar-subtropical coupling processes can substantially modulate the regional expression of anthropogenic warming.

Recent studies using large ensembles and mechanism-denial experiments further indicate that high-latitude processes can influence lower-latitude Pacific climate. Coupled simulations show that SO heat uptake can alter the tropical Pacific mean state and strengthen the Walker circulation (Kang, Shin, et al., 2023), and pacemaker experiments demonstrate that SO cooling can force cooling in the southeastern tropical Pacific through atmospheric teleconnections modulated by subtropical cloud feedbacks (Kang, Yu, et al., 2023; Kim et al., 2022). However, observational evidence for a time-varying and bidirectional linkage between the SO and SEP, including its directionality and persistence, remains limited.

Conventional statistical methods often assume linear and stationary relationships, limiting their ability to disentangle external forcing from internal oceanic persistence (Deser et al., 2010; Kumar & Hoerling, 1998). Coupled climate models frequently underestimate observed regional cooling due to biases in wind, sea-ice, and cloud–radiation feedbacks (Coats & Karnauskas, 2017; Wills et al., 2022).

Here, we integrate nonparametric trend diagnostics with an interpretable machine learning framework to identify the evolving contributors to SST anomalies in the SEP and SO from 1960 to 2024. Our framework explicitly separates the contributions of atmospheric circulation, thermodynamics, and cryospheric processes from oceanic persistence in monthly SST anomalies. We further quantify bidirectional connectivity between the SEP and SO using cross-predictive modeling and examine its evolution in moving multi-decadal windows. This combined analysis yields a physically interpretable perspective on how circulation and sea-ice changes jointly drive recent cooling in both regions and reveals the emergence of an asymmetric, time-varying coupling between the subtropical Southeast Pacific and the high-latitude SO.

2. Data and Methods

2.1. Data Sources and Preprocessing

We analyze sea surface temperature (SST) anomalies from the HadISST1 data set (Rayner et al., 2003) over the Southeast Pacific (SEP; 235°–290°E, 12°–28°S) and Southern Ocean (SO; 190°–250°E, 55°–70°S). Anomalies are computed relative to the 1961–1990 climatology. These serve as the target variables.

The SEP and SO domains were chosen based on the spatial coherence of observed multi-decadal cooling trends (Figure 1). To test robustness, we performed sensitivity analyses using alternative regional definitions, including the southeast Pacific SO region from Dong et al. (2022) and a zonally averaged SO band. The SEP evolution proved insensitive to reasonable boundary changes, whereas the SO mean anomaly was sensitive to longitudinal averaging, reflecting zonal heterogeneity in SO trends (Figure S3 in Supporting Information S1). Our selected SO domain isolates the Pacific-sector cooling signal most dynamically connected to the SEP.

Predictors were selected to represent six physically distinct process categories known to influence regional SST variability: thermodynamic air–sea exchange, large-scale atmospheric circulation, radiation and cloud processes, sea-ice forcing, remote climate modes, and surface wave/precipitation forcing (Table S1 in Supporting Information S1; groupings defined in Table S2 in Supporting Information S1). This physically motivated selection ensures that the major drivers identified in prior studies of SEP and SO climate are represented, while the drop-one-group ablation (Section 2.3.1) directly tests the contribution of each category. ERA5 reanalysis (Hersbach et al., 2020) provides globally consistent fields of circulation, radiation, and cloud variables. Subsurface ocean predictors (temperature and salinity in 0–100 m and 100–300 m layers) came from EN4.2.2 (Good et al., 2013). Large-scale climate modes were represented by standardized indices of the SAM (from British Antarctic Survey, BAS), Niño 3.4 (from NOAA Physical Sciences Laboratory, PSL), Pacific Decadal Oscillation (PDO, from NOAA National Centers for Environmental Information, NCEI), and Indian Ocean Dipole (IOD, from NOAA PSL). Short lags (1–3 months) were applied to ERA5 and EN4 predictors; climate indices were lagged up to 12 months to capture characteristic teleconnection timescales. All data were aligned on a common $1° \times 1°$ grid from 1960 to 2024. SST and its derivatives were excluded from predictors to prevent leakage.

2.2. SST Trend Evolution and SEP–SO Linkages

Long-term SST trends were estimated at each grid point using the trend-free pre-whitened Mann–Kendall test with Sen's slope estimator (Yue et al., 2002a), which reduces the influence of serial autocorrelation and provides a robust estimate of monotonic trend magnitude. Field significance was controlled using the Benjamini–Yekutieli false discovery rate ($q < 0.05$) (D. Wilks, 2006).

Regional average SST anomalies for SEP and SO were smoothed using locally weighted regression (LOWESS) to highlight multi-decadal shifts (Cleveland, 1981; Mudelsee, 2010). Significance of cooling or warming intervals was assessed using moving-block bootstrap confidence intervals that preserve temporal autocorrelation. Monotonic trend evolution was tracked by computing the Mann–Kendall τ statistic in 20-year rolling windows. The 20-year window was chosen to balance temporal resolution against statistical robustness; shorter windows (10 years) are dominated by interannual noise, while longer windows (30 years) obscure the timing of multi-decadal trend reversals (Figure S2 in Supporting Information S1).

To evaluate how coupling between the SEP and SO has changed over time, we computed rolling cross-correlation functions (D. S. Wilks, 2011) in 20-year windows stepped by one year, considering lags from −24 to +24 months. Changes in coupling strength were quantified using rolling Kendall's τ tests (Bretherton et al., 1999). Details are provided in Supporting Information S1 Methods.

2.3. Attribution Using an Interpretable Machine-Learning Framework

Monthly SST anomalies (y_t) exhibit strong persistence due to mixed-layer memory (Alexander & Deser, 1995; Hasselmann, 1976; Monetti et al., 2003), which can inflate apparent predictive skill when predictors co-vary with SST (DelSole & Tippett, 2009; Frankignoul & Hasselmann, 1977). To isolate contemporaneous physical influences external to SST persistence, we analyze SST innovations defined as the month-to-month departure from persistence,

$$r_t = y_t - y_{t-1}. \tag{1}$$

We employ a gradient-boosted regression tree (XGBoost) to model the innovations. This approach captures nonlinear interactions while supporting transparent attribution via SHapley Additive exPlanations (SHAP) values and ablation tests (Hermosilla et al., 2025; Nielsen, 2016; Wu et al., 2023). A gradient-boosted regressor is trained to predict r_t from contemporaneous and lagged physical predictors:

$$\hat{r}_t = g_\phi(\mathbf{x}_t), \tag{2}$$

and predicted anomalies are reconstructed as

$$\hat{y}_t = y_{t-1} + \hat{r}_t. \tag{3}$$

Because the model is fitted to the departures from persistence, any predictive skill must arise from physical predictors that actively modify SST rather than from autocorrelation alone. We implement three complementary configurations to quantify the contribution of physical predictors: (a) a persistence-only baseline, $\hat{y}_t^{\text{pers}} = y_{t-1}$; (b) a predictor-only model that predicts y_t directly from physical predictors; and (c) a persistence-plus-predictors model that predicts innovations r_t and reconstructs anomalies as $y_{t-1} + \hat{r}_t$.

Model performance was evaluated using forward-chaining cross-validation with a 1-month buffer between training and validation blocks. Skill was measured by out-of-fold coefficient of determination (R^2), root-mean-square error (RMSE), and mean absolute error relative to a persistence baseline. Residual autocorrelation (ACF) was examined to ensure that unremoved memory did not inflate skill (Box & Pierce, 1970; Dean & Dunsmuir, 2016) (Detailed algorithmic implementation is provided in Supporting Information S1).

2.3.1. Interpretability Diagnostics

We use two complementary diagnostics to interpret models: (a) SHAP, which decompose predictions into additive contributions from each predictor (because the innovation model is trained on r_t, its SHAP values quantify predictor contributions beyond persistence); and (b) drop-one-group ablation; in which predictors are grouped into physically interpretable process categories (see Table S2 in Supporting Information S1). The grouping is designed for attribution testing and reflects physically interpretable process separation rather than data-driven clustering. For each group G, we recompute out-of-fold RMSE after removing that group and report the penalty ΔRMSE_G. Larger penalties indicate greater explanatory content.

$$\Delta\text{RMSE}_G = \text{RMSE}_{\text{drop}(G)} - \text{RMSE}_{\text{full}}. \tag{4}$$

2.3.2. Cross-Basin Predictive Connectivity

To quantify time-varying bidirectional coupling between the SEP and SO, we extend the innovation framework to a cross-predictive setting. Each basin's innovation series (r_t^{SEP}, r_t^{SO}) is predicted using only predictors from the opposite basin, thereby isolating cross-regional influences independent of local persistence.

The analysis is conducted in overlapping 20-year windows stepped by 10 years across 1960–2024. For each window, lagged predictor matrices (1–6 months lags) are constructed from ERA5, EN4, and climate indices. To ensure robust evaluation, data are split 80/20 into training and testing subsets, with the test set reserved exclusively for final performance assessment and never used for parameter tuning or model selection. Gradient-boosted trees (XGBoost) are trained in two configurations using fixed, conservatively regularized hyperparameters: (a) SEP innovations predicted from SO predictors, and (b) SO innovations predicted from SEP predictors. These hyperparameters were selected through preliminary out-of-fold validation on the full 1960–2024 data set and then held constant across all windows to ensure comparability and prevent overfitting. Model explanatory power was quantified using the coefficient of determination,

$$R^2 = 1 - \frac{\sum_t (y_t - \hat{y}_t)^2}{\sum_t (y_t - \bar{y})^2} \tag{5}$$

calculated on reconstructed SST anomalies $(\hat{y}_t)$ for the test set within each window. To diagnose the underlying mechanisms, mean absolute SHAP values (Lundberg & Lee, 2017) are calculated from test data within each window, retaining the most influential predictors.

3. Results

3.1. Evolution of SST Trends

We first examine the observed evolution of SST trends, which provides the empirical context for attribution. Figure 1 shows the spatial pattern and temporal progression of trends across three sub-periods. Between 1960 and 1980 (Figure 1a), positive trends dominate midlatitude and polar oceans, while the SEP displays weak coastal warming alongside offshore cooling. From 1981 to 2000 (Figure 1b), this pattern reverses, with coherent cooling emerging across the SEP and strengthening in the SO. During 2001–2024 (Figure 1c), basin-scale cooling

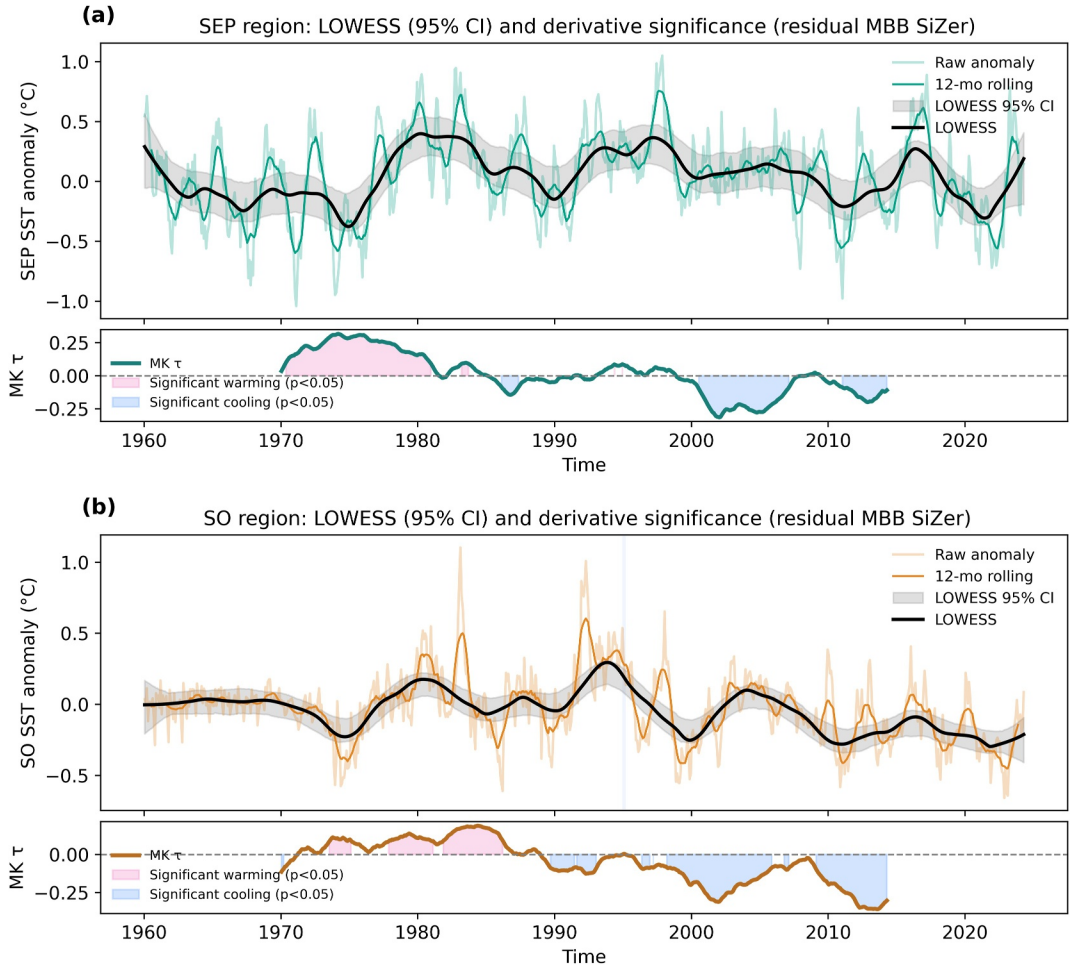

Figure 2. Regional sea surface temperature anomalies for the Southeast Pacific (SEP) and Southern Ocean (SO). (a) SEP and (b) SO. Thin lines show monthly anomalies; thicker lines show 12-month rolling means. The black curve is a LOWESS fit with pointwise 95% confidence bands from a residual moving-block bootstrap (24-month blocks, 800 resamples) on the original time grid. Background shading marks intervals where the simultaneous 95% confidence band for the LOWESS derivative excludes zero (pink = warming, blue = cooling). Lower sub-panels show 20-year rolling Mann–Kendall τ; shading indicates periods with $p < 0.05$.

prevails in both regions. These transitions highlight a non-monotonic, multi-decadal reorganization of Southern Hemisphere SST trends.

The temporal evolution of regional average anomalies (Figure 2) reinforces this spatial pattern. In the SEP, near-neutral or weak cooling prevailed through the late 1960s, followed by modest warming in the 1970s and a relatively flat phase in the 1980s. A sustained, statistically significant cooling regime emerged in the early 2000s and persisted through the 2010s, with only partial rebound in recent years. In the SO, weak variability dominated the 1960s to early 1970s, after which a significant warming interval occurred in the late 1970–1980s. Multi-decadal cooling became the dominant signal from the early 2000s onward. The SEP evolution is robust to reasonable boundary adjustments, whereas the SO temporal trajectory is sensitive to longitudinal averaging due to zonal heterogeneity in trends (Figure S3 in Supporting Information S1). This established temporal structure motivates the subsequent attribution of physical predictors behind the SEP and SO cooling.

3.2. Time-Varying Lead–Lag Correlations Between SEP and SO

The relationship between SEP and SO SST anomalies is neither stationary in strength nor fixed in direction (Figure 3). During the 1970–1980s, correlations peaked near zero lag, indicating largely synchronous variability. From the late 1980s onward, the peak significant correlations shifted from lag 0 to lag −1 to −2 months,

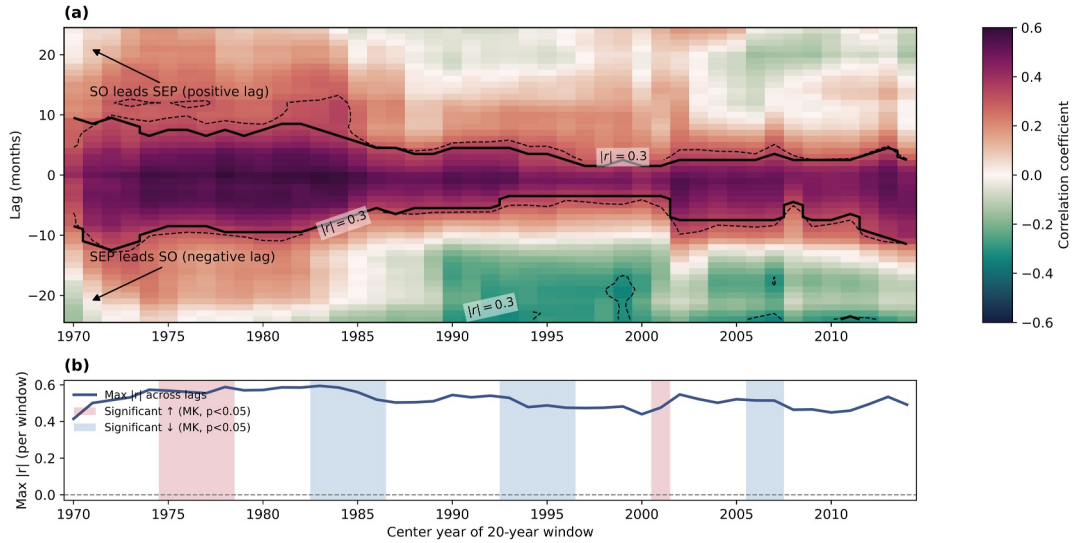

Figure 3. Time-evolving lead–lag correlations between SEP and Southern Ocean (SO) sea surface temperature anomalies. (a) Pearson correlations computed in 20-year windows (stepped by 12 months) for lags from −24 to +24 months (positive values indicate SO leads SEP; negative values indicate SEP leads SO). The solid contour marks grid points that are significant at $p < 0.05$, accounting for AR (1) autocorrelation using window-specific effective sample sizes; the dashed contour marks the heuristic strength level $|r| = 0.3$. (b) Maximum absolute correlation per window, $\max_{\ell}|r(\ell)|$, with shading where a 10-year rolling Kendall's τ detects significant increases (red) or decreases (blue) at $p < 0.05$.

indicating near-synchronous covariability in which SEP changes marginally lead those in the SO. In windows centered in the mid-2000s, significant correlations extended to lags of −4 to −7 months, suggesting episodes where SEP variability preceded that in the SO at subannual timescales. The lower panel of Figure 3 indicates that the overall strength of the SEP–SO coupling varied non-monotonically, with significant increases and decreases over successive decades.

3.3. Attribution of SST Anomalies

Model evaluation (out-of-fold performance, described in Supporting Information S1) indicates that monthly SST variability in both regions is dominated by upper-ocean persistence, while physical predictors provide additional but smaller explanatory power. The innovation framework isolates the contribution of contemporaneous processes beyond autoregressive memory.

Process-group ablation (Figure 4) and SHAP attribution (Figure 5) reveal regionally distinct controlling mechanisms. In the SEP, radiation–cloud effects and thermodynamics are the dominant contributors beyond persistence. In the SO, sea-ice concentration, subsurface temperature, and large-scale circulation play leading roles. Removing persistence substantially reduces the apparent importance of most predictors (ΔRMSE on the order of 10^{-3} °C), suggesting that the innovation formulation effectively isolates active forcing from co-variability.

Feature-level SHAP rankings (Figure 5) further clarify these contrasts. In the SEP, low- and mid-level cloud cover, surface shortwave radiation, and the Antarctic Oscillation provide the strongest contributions beyond persistence, consistent with local air–sea thermodynamic feedbacks. In the SO, sea-ice concentration, near-surface temperature, and high-latitude circulation variables dominate, highlighting cryospheric and dynamically driven variability. Together, these diagnostics indicate that SEP variability is governed mainly by local thermodynamic–radiative coupling, whereas SO variability reflects coupled atmosphere–ocean–ice processes.

3.3.1. Cross-Basin Connectivity Between SEP and SO

Cross-predictive R^2 values for reconstructed SST anomalies (Figure 6) reveal robust but time-dependent coupling between the two basins. The SO → SEP direction maintains consistently higher predictive skill ($R^2 \approx 0.7$–0.8), indicating that SO anomalies provide stable information for predicting subsequent SST changes in the Southeast Pacific. The reverse SEP → SO pathway shows lower and more variable skill, peaking near 0.8 around the 1990s

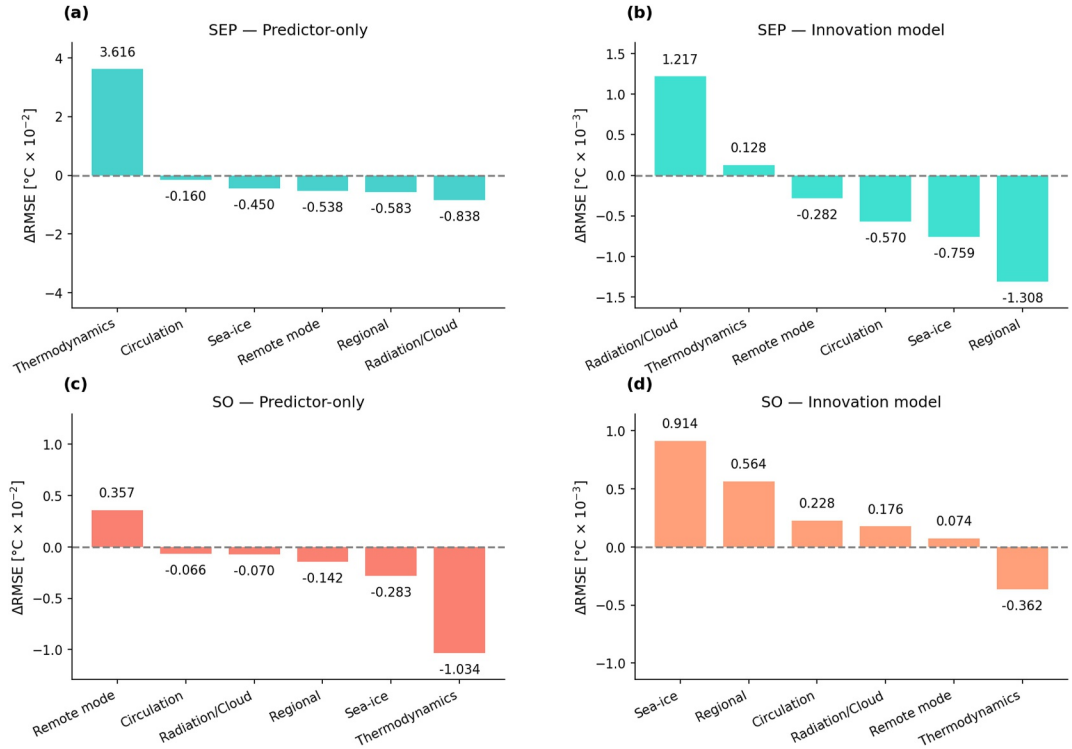

Figure 4. Process-group ablation penalties $(\Delta\text{RMSE} = \text{RMSE}_{\text{drop}} - \text{RMSE}_{\text{full}})$ for the Southeast Pacific (top row) and Southern Ocean (SO) (bottom row). (a) SEP predictor-only model, (b) SEP innovation model, (c) SO predictor-only model, (d) SO innovation model. Positive values indicate reduced skill when a process group is removed.

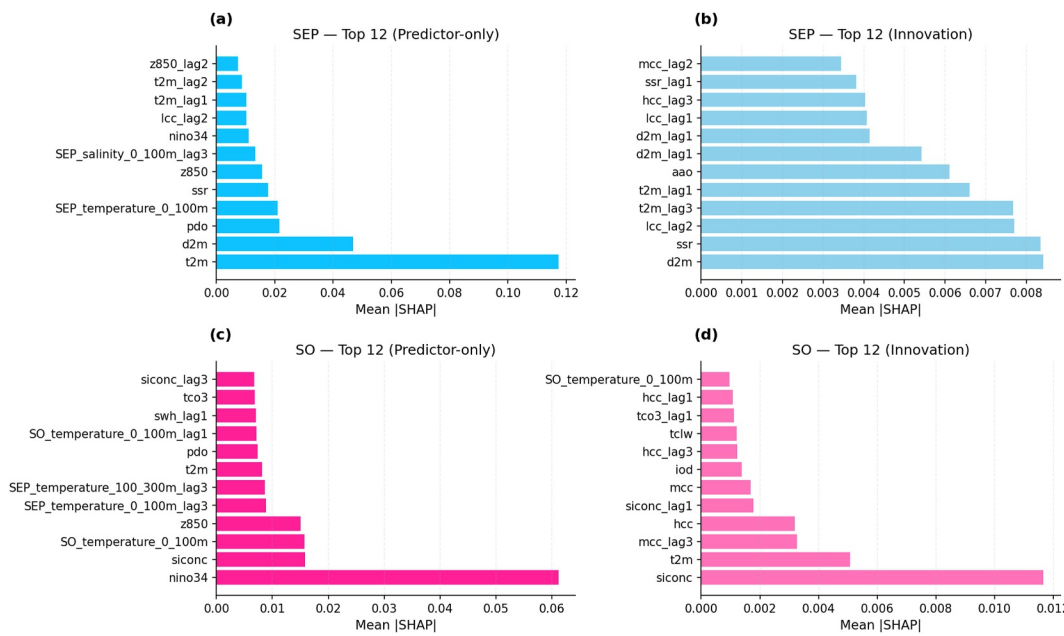

Figure 5. Top 12 predictors ranked by mean absolute SHAP values for the Southeast Pacific (SEP; top row) and Southern Ocean (SO; bottom row). (a) SEP predictor-only model, (b) SEP innovation model, (c) SO predictor-only model, (d) SO innovation model. Predictor abbreviations are defined in Table S1 in Supporting Information S1.

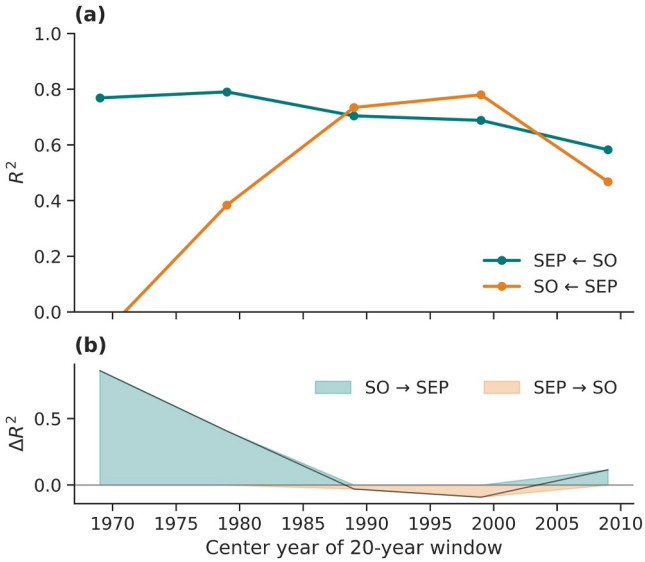

Figure 6. Temporal evolution of SEP–SO cross-basin connectivity. (a) Cross-validated coefficient of determination (R^2) for each direction in overlapping 20-year windows, computed on reconstructed sea surface temperature anomalies $(\hat{y}_t = y_{t-1} + \hat{r}_t)$ from cross-basin innovation models. (b) Difference (ΔR^2) showing the relative dominance of the SO → SEP (cyan) or SEP → SO (orange) direction.

before declining after 2000. This asymmetry demonstrates that the coupling is not reciprocal: the dominant direction of influence is from south to north.

The temporal evolution of R^2 asymmetry aligns with the lead–lag correlation patterns in Figure 3: when SO → SEP R^2 exceeds the reverse, correlations peak at positive lags (SO leads), whereas near the 1990s peak in SEP → SO R^2, correlations shift to zero or weakly negative lags. Elevated SEP→SO skill in the late-1990s to early-2000s windows coincides with the final stage of the positive PDO phase (~1977–1998), when tropical Pacific variability may have influenced both basins. SHAP diagnostics (Figure S6 in Supporting Information S1) indicate that Niño 3.4 and the IOD are leading predictors in the SO ← SEP direction mainly in those windows; after the PDO transitioned to its negative phase, these tropical predictors became less prominent and SEP → SO skill declined, consistent with a re-emergence of the stronger SO → SEP asymmetry.

Temporal SHAP diagnostics (Figure S6 in Supporting Information S1) provide mechanistic context for the coupling asymmetry. For the SEP ← SO direction, large-scale circulation and cloud–radiative predictors (Antarctic Oscillation, mid-level cloud cover, 500 hPa geopotential height) remain consistently important across most windows. For the SO ← SEP direction, tropical predictors (Niño 3.4, IOD) appear intermittently, suggesting that the SEP → SO linkage may be modulated by the background state of Pacific decadal variability. Sensitivity tests using the Dong et al. (2022) SO domain yield qualitatively consistent results, indicating that the asymmetric coupling is robust to the choice of SO region (Figure S8 in Supporting Information S1).

These diagnostics identify time-varying statistical associations that are consistent with tropical/PDO modulation of the SEP → SO pathway, but they do not by themselves establish a causal mechanism.

4. Summary and Discussion

Our analysis demonstrates that monthly SST variability in the Southeast Pacific (SEP) and SO is dominated by upper-ocean persistence but modulated by distinct physical processes in each region. Beyond persistence, SEP variability is primarily associated with local thermodynamic and cloud–radiative interactions, whereas SO variability is primarily associated with sea-ice variability and high-latitude circulation, with remote climate modes providing a secondary, time-dependent contribution.

The cross-basin analysis reveals asymmetric and time-dependent coupling, with SO variability providing a stronger and more persistent source of information for SEP SST changes. The SEP → SO pathway appears to be associated with tropical climate modes (Niño 3.4, IOD) during the positive PDO phase (~1977–1998), when these predictors are most prominent in the SO ← SEP SHAP diagnostics and SEP → SO connectivity is strongest (Figures S6 and S7 in Supporting Information S1). After the PDO turned negative, these predictors became less prominent and SEP → SO connectivity declined. This co-evolution is consistent with tropical/PDO modulation of the pathway, although the present framework does not by itself establish causality. By contrast, the SO→SEP pathway is associated with atmospheric circulation and cloud–radiative processes that remain important regardless of the PDO state.

These observational results support a recently hypothesized cloud-mediated teleconnection pathway from the SO to the subtropical Pacific. The dominance of the SO → SEP influence is consistent with pacemaker simulations showing that SO cooling can induce cooling in the southeastern tropical Pacific (Kang, Yu, et al., 2023). This atmospheric pathway does not require spatially continuous surface cooling between the SO and SEP; the intervening warm zone visible in Figures 1b and 1c is consistent with atmospheric circulation and cloud–radiative adjustments acting as the primary bridge between the two regions (Kim et al., 2022). Physically, SO cooling strengthens the meridional temperature gradient, which shifts the subtropical jet and the South Pacific high, thereby enhancing coastal upwelling and modifying low-level cloud cover over the SEP. The importance of cloud and shortwave radiative variability in the SEP agrees with the mechanism proposed by Kim et al. (2022), in which

subtropical stratocumulus feedbacks amplify this high-latitude forcing. Our results provide observational evidence that this mechanism operates in the coupled system and varies over time.

Our current framework has limitations. The analysis relies on reanalysis and observational products with approximately 1° resolution that do not resolve mesoscale ocean eddies, which may contribute to SO heat redistribution. Recent high-resolution modeling studies suggest that eddy-resolving simulations better reproduce observed cooling trends in the SO and SEP, highlighting the role of mesoscale processes in modulating heat transport and sea-ice variability (Kang et al., 2026). Incorporating such eddy-rich dynamics may further refine estimates of SO → SEP coupling strength and clarify whether mesoscale processes amplify or dampen the asymmetric teleconnection identified here.

Overall, the results indicate that SEP–SO coupling is both asymmetric and temporally evolving, with high-latitude variability exerting a sustained influence on subtropical SST variability. This highlights a broader role for SO processes in modulating regional expressions of global warming and suggests that changes in circulation, sea ice, and cloud feedbacks can redistribute heat across latitudes rather than simply alter the global mean state.

Inclusion in Global Research Statement

This research used exclusively publicly available global observational and reanalysis data sets and did not involve fieldwork, data collection, or engagement with local communities. No additional permits or local authorizations were required.

Conflict of Interest

The authors declare no conflicts of interest relevant to this study.

Availability Statement

Sea surface temperature data from HadISST1 are publicly available from the Met Office Hadley Centre (https://www.metoffice.gov.uk/hadobs/hadisst/).

EN4 subsurface ocean data are provided by the UK Met Office (https://www.metoffice.gov.uk/hadobs/en4/).

ERA5 reanalysis data were obtained from the Copernicus Climate Data Store: monthly averaged single-level fields (Hersbach et al., 2023b) (https://doi.org/10.24381/cds.f17050d7) and monthly averaged pressure-level fields (Hersbach et al., 2023a) (https://doi.org/10.24381/cds.6860a573).

The SAM index is available from the British Antarctic Survey (https://legacy.bas.ac.uk/met/gjma/sam.html). The PDO index is available from NOAA NCEI (https://www.ncei.noaa.gov/access/monitoring/pdo/). The Niño 3.4 and IOD indices are available from NOAA PSL (https://psl.noaa.gov/data/timeseries/month/DS/Nino34/, https://psl.noaa.gov/data/timeseries/month/DMI/).

The analysis scripts supporting this study are archived on Zenodo (Hu, 2026). All observational and reanalysis data sets used in this study are publicly available from the sources listed above.

Acknowledgments
X.H. was supported by the Calleva Research Centre through the project "Climate Change: Effects and Solutions." L.S. was supported by UKRI (UKRI2054).

References

Alexander, M. A., & Deser, C. (1995). A mechanism for the recurrence of wintertime midlatitude sst anomalies. *Journal of Physical Oceanography*, *25*(1), 122–137. https://doi.org/10.1175/1520-0485(1995)025<0122:amftro>2.0.co;2

Armour, K. C., Marshall, J., Scott, J. R., Donohoe, A., & Newsom, E. R. (2016). Southern Ocean warming delayed by circumpolar upwelling and equatorward transport. *Nature Geoscience*, *9*(7), 549–554. https://doi.org/10.1038/ngeo2731

Box, G. E., & Pierce, D. A. (1970). Distribution of residual autocorrelations in autoregressive-integrated moving average time series models. *Journal of the American Statistical Association*, *65*(332), 1509–1526. https://doi.org/10.1080/01621459.1970.10481180

Boyd, P. W., Arrigo, K. R., Ardyna, M., Halfter, S., Huckstadt, L., Kuhn, A. M., et al. (2024). The role of biota in the Southern Ocean carbon cycle. *Nature Reviews Earth and Environment*, *5*(5), 390–408. https://doi.org/10.1038/s43017-024-00531-3

Bretherton, C. S., Widmann, M., Dymnikov, V. P., Wallace, J. M., & Bladé, I. (1999). The effective number of spatial degrees of freedom of a time-varying field. *Journal of Climate*, *12*(7), 1990–2009. https://doi.org/10.1175/1520-0442(1999)012<1990:tenosd>2.0.co;2

Caldeira, K., & Duffy, P. B. (2000). The role of the Southern Ocean in uptake and storage of anthropogenic carbon dioxide. *Science*, *287*(5453), 620–622. https://doi.org/10.1126/science.287.5453.620

Cerovečki, I., Meijers, A. J., Mazloff, M. R., Gille, S. T., Tamsitt, V. M., & Holland, P. R. (2019). The effects of enhanced sea ice export from the Ross Sea on recent cooling and freshening of the Southeast Pacific. *Journal of Climate*, *32*(7), 2013–2035. https://doi.org/10.1175/jcli-d-18-0205.1

Chavez, F., Bertrand, A., Guevara-Carrasco, R., Soler, P., & Csirke, J. (2008). The northern Humboldt Current system: Ocean dynamics, ecosystem processes, and fisheries. *Progress in Oceanography*, *79*, 95–105.

Cleveland, W. S. (1981). Lowess: A program for smoothing scatterplots by robust locally weighted regression. *The American Statistician*, *35*(1), 54. https://doi.org/10.2307/2683591

Coats, S., & Karnauskas, K. (2017). Are simulated and observed twentieth century tropical Pacific sea surface temperature trends significant relative to internal variability? *Geophysical Research Letters*, *44*(19), 9928–9937. https://doi.org/10.1002/2017gl074622

Dean, R. T., & Dunsmuir, W. T. (2016). Dangers and uses of cross-correlation in analyzing time series in perception, performance, movement, and neuroscience: The importance of constructing transfer function autoregressive models. *Behavior Research Methods*, *48*(2), 783–802. https://doi.org/10.3758/s13428-015-0611-2

DelSole, T., & Tippett, M. K. (2009). Average predictability time. Part II: Seamless diagnoses of predictability on multiple time scales. *Journal of the Atmospheric Sciences*, *66*(5), 1188–1204. https://doi.org/10.1175/2008jas2869.1

Deser, C., Alexander, M. A., Xie, S.-P., & Phillips, A. S. (2010). Sea surface temperature variability: Patterns and mechanisms. *Annual Review of Marine Science*, *2*(1), 115–143. https://doi.org/10.1146/annurev-marine-120408-151453

Dong, Y., Armour, K. C., Battisti, D. S., & Blanchard-Wrigglesworth, E. (2022). Two-way teleconnections between the Southern Ocean and the tropical Pacific via a dynamic feedback. *Journal of Climate*, *35*(19), 6267–6282. https://doi.org/10.1175/jcli-d-22-0080.1

Falvey, M., & Garreaud, R. D. (2009). Regional cooling in a warming world: Recent temperature trends in the southeast Pacific and along the West Coast of subtropical South America (1979–2006). *Journal of Geophysical Research*, *114*(D4), D04102. https://doi.org/10.1029/2008jd010519

Frankignoul, C., & Hasselmann, K. (1977). Stochastic climate models, part ii application to sea-surface temperature anomalies and thermocline variability. *Tellus*, *29*(4), 289–305. https://doi.org/10.1111/j.2153-3490.1977.tb00740.x

Garreaud, R. D., Clem, K., & Veloso, J. V. (2021). The south Pacific pressure trend dipole and the southern blob. *Journal of Climate*, *34*(18), 7661–7676. https://doi.org/10.1175/jcli-d-20-0886.1

Good, S. A., Martin, M. J., & Rayner, N. A. (2013). En4: Quality controlled ocean temperature and salinity profiles and monthly objective analyses with uncertainty estimates. *Journal of Geophysical Research: Oceans*, *118*(12), 6704–6716. https://doi.org/10.1002/2013jc009067

Gruber, N., Bakker, D. C., DeVries, T., Gregor, L., Hauck, J., Landschützer, P., et al. (2023). Trends and variability in the ocean carbon sink. *Nature Reviews Earth and Environment*, *4*(2), 119–134. https://doi.org/10.1038/s43017-022-00381-x

Hasselmann, K. (1976). Stochastic climate models part I. Theory. *Tellus*, *28*(6), 473–485. https://doi.org/10.3402/tellusa.v28i6.11316

Hermosilla, P., Berríos, S., & Allende-Cid, H. (2025). Explainable ai for forensic analysis: A comparative study of shap and lime in intrusion detection models. *Applied Sciences*, *15*(13), 7329. https://doi.org/10.3390/app15137329

Hersbach, H., Bell, B., Berrisford, P., Biavati, G., Horányi, A., Muñoz Sabater, J., et al. (2023a). Era5 monthly averaged data on pressure levels from 1940 to present [dataset]. *Copernicus Climate Change Service (C3S) Climate Data Store (CDS)*. https://doi.org/10.24381/cds.6860a573

Hersbach, H., Bell, B., Berrisford, P., Biavati, G., Horányi, A., Muñoz Sabater, J., et al. (2023b). Era5 monthly averaged data on single levels from 1940 to present [dataset]. *Copernicus Climate Change Service (C3S) Climate Data Store (CDS)*. https://doi.org/10.24381/cds.f17050d7

Hersbach, H., Bell, B., Berrisford, P., Hirahara, S., Horányi, A., Muñoz-Sabater, J., et al. (2020). The era5 global reanalysis. *Quarterly journal of the royal meteorological society*, *146*(730), 1999–2049. https://doi.org/10.1002/qj.3803

Hu, X. (2026). Analysis scripts for asymmetric ocean–atmosphere coupling between southeast Pacific and Southern Ocean cooling through circulation and sea-ice changes [software]. *Zenodo*. https://doi.org/10.5281/zenodo.20600339

Kang, S. M., Ceppi, P., Yu, Y., & Kang, I.-S. (2023c). Recent global climate feedback controlled by Southern Ocean cooling. *Nature Geoscience*, *16*(9), 775–780. https://doi.org/10.1038/s41561-023-01256-6

Kang, S. M., Putrasahan, D. A., Brizuela, N. G., Haak, H., Kröger, J., Marotzke, J., et al. (2026). Km-scale coupled simulation and model–observation sst trend discrepancy. *Proceedings of the National Academy of Sciences*, *123*(8), e2522161123. https://doi.org/10.1073/pnas.2522161123

Kang, S. M., Shin, Y., Kim, H., Xie, S.-P., & Hu, S. (2023a). Disentangling the mechanisms of equatorial Pacific climate change. *Science Advances*, *9*(19), eadf5059. https://doi.org/10.1126/sciadv.adf5059

Kang, S. M., Yu, Y., Deser, C., Zhang, X., Kang, I.-S., Lee, S.-S., et al. (2023b). Global impacts of recent Southern Ocean cooling. *Proceedings of the National Academy of Sciences*, *120*(30), e2300881120. https://doi.org/10.1073/pnas.2300881120

Kim, H., Kang, S. M., Kay, J. E., & Xie, S.-P. (2022). Subtropical clouds key to Southern Ocean teleconnections to the tropical Pacific. *Proceedings of the National Academy of Sciences*, *119*(34), e2200514119. https://doi.org/10.1073/pnas.2200514119

Kumar, A., & Hoerling, M. P. (1998). Annual cycle of pacific–north American seasonal predictability associated with different phases of enso. *Journal of Climate*, *11*(12), 3295–3308. https://doi.org/10.1175/1520-0442(1998)011<3295:acopna>2.0.co;2

Landschützer, P., Gruber, N., Haumann, F. A., Rödenbeck, C., Bakker, D. C., Van Heuven, S., et al. (2015). The reinvigoration of the Southern Ocean carbon sink. *Science*, *349*(6253), 1221–1224. https://doi.org/10.1126/science.aab2620

Lundberg, S. M., & Lee, S.-I. (2017). A unified approach to interpreting model predictions. *Advances in Neural Information Processing Systems*, *30*.

Marshall, G. J. (2003). Trends in the southern annular mode from observations and reanalyses. *Journal of Climate*, *16*(24), 4134–4143. https://doi.org/10.1175/1520-0442(2003)016<4134:titsam>2.0.co;2

Mayewski, P. A., Meredith, M., Summerhayes, C., Turner, J., Worby, A., Barrett, P., et al. (2009). State of the Antarctic and Southern Ocean climate system. *Reviews of Geophysics*, *47*(1), RG1003. https://doi.org/10.1029/2007rg000231

Monetti, R. A., Havlin, S., & Bunde, A. (2003). Long-term persistence in the sea surface temperature fluctuations. *Physica A: Statistical Mechanics and its Applications*, *320*, 581–589. https://doi.org/10.1016/s0378-4371(02)01662-x

Mudelsee, M. (2010). Climate time series analysis. *Atmospheric and*, 397.

Nielsen, D. (2016). *Tree boosting with xgboost-why does xgboost win" every" machine learning competition? (master's thesis*. Norwegian University of Science and Technology (NTNU). Retrieved from https://ntnuopen.ntnu.no/ntnu-xmlui/handle/11250/2433761

Pennington, J. T., Mahoney, K. L., Kuwahara, V. S., Kolber, D. D., Calienes, R., & Chavez, F. P. (2006). Primary production in the eastern tropical Pacific: A review. *Progress in Oceanography*, *69*(2–4), 285–317. https://doi.org/10.1016/j.pocean.2006.03.012

Qiu, W., Collins, M., Scaife, A. A., & Santoso, A. (2024). Tropical Pacific trends explain the discrepancy between observed and modelled rainfall change over the Americas. *NPJ Climate and Atmospheric Science*, *7*(1), 201. https://doi.org/10.1038/s41612-024-00750-x

Rayner, N. A., Parker, D. E., Horton, E., Folland, C. K., Alexander, L. V., Rowell, D., et al. (2003). Global analyses of sea surface temperature, sea ice, and night marine air temperature since the late nineteenth century. *Journal of Geophysical Research*, *108*(D14), 4407. https://doi.org/10.1029/2002jd002670

Sallée, J.-B., Abrahamsen, E. P., Allaigre, C., Auger, M., Ayres, H., Badhe, R., et al. (2023). Southern Ocean carbon and heat impact on climate. *Philosophical Transactions of the Royal Society A: Mathematical, Physical and Engineering Sciences*, *381*(2249), 20220056. https://doi.org/10.1098/rsta.2022.0056

Seager, R., Henderson, N., Cane, M., Zhang, H., & Nakamura, J. (2021). Atmosphere–ocean dynamics of persistent cold states of the tropical Pacific Ocean. *Journal of Climate*, *34*(13), 5195–5214. https://doi.org/10.1175/jcli-d-20-0694.1

Wilks, D. (2006). On "field significance" and the false discovery rate. *Journal of Applied Meteorology and Climatology*, *45*(9), 1181–1189. https://doi.org/10.1175/jam2404.1

Wilks, D. S. (2011). *Statistical methods in the atmospheric sciences* (Vol. 100). Academic Press.

Wills, R. C., Dong, Y., Proistosecu, C., Armour, K. C., & Battisti, D. S. (2022). Systematic climate model biases in the large-scale patterns of recent sea-surface temperature and sea-level pressure change. *Geophysical Research Letters*, *49*(17), e2022GL100011. https://doi.org/10.1029/2022gl100011

Wu, Z., Zhu, J., Li, Q., & He, B. (2023). Deltaboost: Gradient boosting decision trees with efficient machine unlearning. *Proceedings of the ACM on Management of Data*, *1*(2), 1–26. https://doi.org/10.1145/3589313

Xu, X., Liu, J., & Huang, G. (2022). Understanding sea surface temperature cooling in the central-east Pacific sector of the Southern Ocean during 1982–2020. *Geophysical Research Letters*, *49*(10), e2021GL097579. https://doi.org/10.1029/2021gl097579

Yue, S., Pilon, P., Phinney, B., & Cavadias, G. (2002a). The influence of autocorrelation on the ability to detect trend in hydrological series. *Hydrological Processes*, *16*(9), 1807–1829. https://doi.org/10.1002/hyp.1095

References From the Supporting Information

Benjamini, Y., & Yekutieli, D. (2001). The control of the false discovery rate in multiple testing under dependency. *Annals of Statistics*, 1165–1188.

Blain, G. C. (2014). Removing the influence of the serial correlation on the mann-kendall test. *Revista Brasileira de Meteorologia*, *29*(2), 161–170. https://doi.org/10.1590/s0102-77862014000200002

Hamed, K. H. (2008). Trend detection in hydrologic data: The mann–kendall trend test under the scaling hypothesis. *Journal of hydrology*, *349*(3–4), 350–363. https://doi.org/10.1016/j.jhydrol.2007.11.009

Helsel, D. R., & Hirsch, R. M. (1993). *Statistical methods in water resources* (Vol. 49). Elsevier.

Hirsch, R. M., Slack, J. R., & Smith, R. A. (1982). Techniques of trend analysis for monthly water quality data. *Water Resources Research*, *18*(1), 107–121. https://doi.org/10.1029/wr018i001p00107

Sen, P. K. (1968). Estimates of the regression coefficient based on kendall's tau. *Journal of the American Statistical Association*, *63*(324), 1379–1389. https://doi.org/10.1080/01621459.1968.10480934

Ventura, V., Paciorek, C. J., & Risbey, J. S. (2004). Controlling the proportion of falsely rejected hypotheses when conducting multiple tests with climatological data. *Journal of Climate*, *17*(22), 4343–4356. https://doi.org/10.1175/3199.1

Yue, S., Pilon, P., Phinney, B., & Cavadias, G. (2002b). Patterns of trend in Canadian streamflow. In *Proceedings if the 58th annual eastern snow conference, gcu, May*.

Yue, S., Pilon, P., & Cavadias, G. (2002c). Power of the mann–kendall and spearman's rho tests for detecting monotonic trends in hydrological series. *Journal of hydrology*, *259*(1–4), 254–271. https://doi.org/10.1016/s0022-1694(01)00594-7